ACS APPLIED BIO MATERIALS

www.acsabm.org

Article

Influence of Lysine and TRITC Conjugation on the Size and Structure of Dextran Nanoconjugates with Potential for Biomolecule Delivery to Neurons

Darya Zeini, Joel C. Glover,* Kenneth D. Knudsen, and Bo Nyström*

Cite This: *ACS Appl. Bio Mater.* 2021, 4, 6832−6842

Read Online

ACCESS | Metrics & More | Article Recommendations | Supporting Information

ABSTRACT: As a potent nonviral system for biomolecular delivery to neurons via their axons, we have studied molecular characteristics of lysinated fluorescent dextran nanoconjugates with degrees of conjugation of 0.54−15.2 mol lysine and 0.25−7.27 mol tetramethyl rhodamine isothiocyanate (TRITC) per mol dextran. We studied the influence of conjugation with lysine and TRITC on the size and structure of different molecular weight dextrans and their mobility within axons. Dynamic light scattering (DLS) and small-angle neutron scattering (SANS) experiments revealed significant differences in the size and structure of unmodified and modified dextrans. Unexpectedly, lower-molecular-weight conjugated dextrans exhibited higher molecular volumes, which we propose is due to fewer intramolecular interactions than in higher-molecular-weight conjugated dextrans. Assessment of retrograde and anterograde movement of lysine- and TRITC-conjugated dextrans in axons in the lumbar spinal cord of chicken embryos showed that lower-molecular-weight dextrans translocate more efficiently than higher-molecular-weight dextrans, despite having larger molecular volumes. This comparative characterization of different molecular weight dextrans will help define optimal features for intracellular delivery.

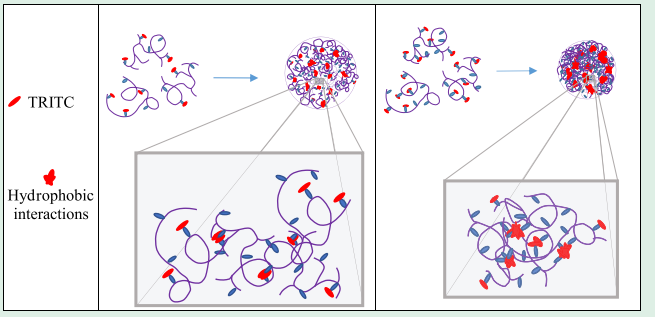

KEYWORDS: *conjugated dextran, axonal transport, retrograde tracing, anterograde tracing, DLS, SANS*

INTRODUCTION

Dextran-based polymers have received great interest for controlled drug release and gene transfection applications.[1−7] Targeted and localized delivery systems based on dextran polymers have several benefits such as high aqueous solubility, high chemical stability, target site specificity, few deleterious effects on cellular function, suitability for programmed release applications, good patient compliance, and high overall efficiency.[8−11] For example, one limitation to the use of nucleic acids for studies of normal and pathophysiological processes and for the potential treatment of neurological disease is the specificity, with which they can be delivered to selected neuron populations.[11,12] This problem can be solved while simultaneously avoiding the risks inherent in using viral carriers using a suitable nonviral polymeric nanocarrier.[12,13] Selectively localized injection of a suitable polymeric nanocarrier can restrict intracellular accumulation to neurons that project to a specific target. For example, motoneurons innervating a specific muscle can be targeted with exquisite selectivity, as can cortical neurons projecting to a specific subcortical target, or thalamic neurons projecting to a specific cortical region, and so on.[14]

Dextran is a natural, biodegradable, and biocompatible nonionic polysaccharide, widely employed for biomedical applications.[15−22] The chemical structure of dextran consists mainly of α-(1 → 6) glycosidic bonds with branching at positions α-(1 → 2), α-(1 → 3), and α-(1 → 4).[9,13,23] The degree of branching in dextran polymers is related to the molecular weight of dextran[24] and is usually pronounced for high molecular weights.

A large number of hydroxyl groups available on the dextran backbone makes the polymer suitable for conjugation with a variety of other molecules with specific characteristics.[25−31] Different chemical reactions, such as esterification, amidation, and oxidation can be used to introduce various functional groups.[13] Based on a protocol established by Gimlich,[32] we used lysine to functionalize the dextran backbone with free amine groups providing (1) further attachment with tetramethyl rhodamine isothiocyanate (TRITC) and (2) later fixation in tissues using aldehyde-mediated condensation.

Received: May 10, 2021
Accepted: August 9, 2021
Published: August 23, 2021

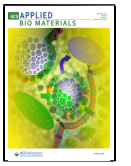

Lysine is selected because of its biocompatibility and biodegradability,[33] its ease of attachment to the dextran backbone,[32] and its provision of another free amine group for further reactions. TRITC is the amine-reactive derivative of the hydrophobic fluorescent dye tetramethyl rhodamine[34] and has been utilized extensively to fluorescently label proteins (such as antibodies) and to label cells when encapsulated or conjugated to other molecules.

The most important feature of dextran that makes it attractive for use in biomolecule delivery in the nervous system is that conjugated dextran can be taken up by axons or synapses and moves retrogradely and anterogradely to neuronal cell bodies and to the synaptic terminals.[35−37] Thus, it can be used as a nonviral nanocarrier delivery system for targeting specific neuron populations.

In this work, we synthesized lysine- and TRITC-conjugated dextrans of three different molecular weights and investigated the effect of the degree of conjugation on the size and structure of the polymer and on the rate and efficiency of movement within axons. We synthesized lysine-conjugated dextran by cyanogen bromide activation of dextran and then attached TRITC to the free amine groups provided by the lysine moieties.[32] Conjugation with TRITC permits the live monitoring of polymer location and movement using fluorescence microscopy. We prepared aqueous solutions of the conjugated dextran polymers and characterized nanostructure and cellular behavior with the aid of NMR, DLS, SANS, and fluorescence microscopy.

The aim of this work is to gain insight into factors that can control the delivery of dextran conjugates to neurons via their axons. A novel feature of this study is to elucidate how the molecular weight of dextran and the lysine and TRITC conjugation affect the mobility of nonvirial carriers. This information is important to understand how cellular uptake and intracellular mobility are affected by these chemical modifications. In this way, we can tailor-make the carriers for optimal performance.

EXPERIMENTAL SECTION

Materials. Dextrans with different weight-average molecular weights (M_w) of 3500 Da (Dex3) and 10 000 Da (Dex10) were purchased from Pharmacosmos (Denmark) and dextran with a M_w of 40 000 Da (Dex40) was obtained from AppliChem (GmbH, Germany). Cyanogen bromide, TRITC, and all other chemicals were obtained from Sigma-Aldrich.

Preparation of Conjugated Dextrans. The dextrans (Dex3, Dex10, and Dex40) were conjugated with different amounts of lysine by cyanogen bromide activation. TRITC was then covalently attached to the lysine moieties in the dextran backbone. Six samples with different degrees of lysine conjugation (Dex3-L1, Dex3-L2, Dex10-L1, Dex10-L2, Dex40-L1, and Dex40-L2) were prepared by the method of Gimlich.[32] The degree of lysine conjugation was tuned by the amount of cyanogen bromide and lysine in the solution (Table 1).

Briefly, the reaction was carried out by dissolving 100 mg of dextran samples (Dex3, Dex10, and Dex40) in 20 mL of distilled water, followed by dropwise addition of 1 N NaOH until the pH reached a value of 10.8. Cyanogen bromide (25 mg) was then added to the solution to produce highly reactive cyanate ester and slightly reactive imidocarbonate intermediates. By adding small volumes of 1 N sodium hydroxide, the pH of the solution was kept constant until the reaction was complete. Cyanate ester reacts readily with primary amine groups of lysine, of which 170 mg was added to the solution along with 370 mg of sodium bicarbonate. The pH was adjusted to 8.4 by adding a few drops of 0.1 N HCl to favor the activity of the α-amino group, which has a pK_a of 8.95, rather than the ε-amino group, which has a pK_a of 10.5. The reaction mixture was then gently stirred for 16 h at 4 °C in a shaking incubator. The solution was thereafter dialyzed against distilled water for 7 days and finally lyophilized (samples labeled as "L1"). This procedure was performed a second time with a twofold increase in the amount of cyanogen bromide and lysine. This led to a near doubling of the degree of conjugation of lysine (samples labeled as "L2").

Table 1. Preparation of Lysine-Conjugated Dextran with Different Feed Ratios of Lysine and Cyanogen Bromide

sample	Dex (M_w)	Dex (mg)	lysine (mg)	cyanogen bromide (mg)
Dex3-L1	3500	100	370	25
Dex3-L2	3500	100	740	50
Dex10-L1	10 000	100	370	25
Dex10-L2	10 000	100	740	50
Dex40-L1	40 000	100	370	25
Dex40-L2	40 000	100	740	50

To attach the TRITC, 60 mg of each lysine-conjugated sample was dissolved in 2 mL of carbonate buffer (pH 9). TRITC (10 mg) was dissolved in 0.5 mL of DMF, followed by the addition of 1 mL of carbonate buffer (pH 9). TRITC solutions were mixed with lysine-conjugated dextran solutions while stirring. The reaction mixture was stirred for 2 h at 40 °C and then dialyzed against carbonate buffer (pH 9) for 2 days, followed by dialyzing against distilled water for 12 days. The resultant samples (Dex3-L1-R, Dex3-L2-R, Dex10-L1-R, Dex10-L2-R, Dex40-L1-R, and Dex40-L2-R) were finally lyophilized and stored at −20 °C until further analysis. Scheme 1 shows the schematic illustration of the synthesis.

For the characterization of dextrans and the conjugates with different experimental techniques, the dry samples were dissolved in D_2O and the solutions were homogenized by magnetic stirring for a day prior to measurements.

^{1}H NMR Spectroscopy. The chemical composition of conjugated dextran was confirmed by proton nuclear magnetic resonance (^{1}H NMR) spectroscopy using a 400 MHz (Bruker AVIII400) instrument at the Department of Chemistry, University of Oslo. Solutions were prepared by dissolving 10 mg of the dry samples in 0.5 mL of D_2O, and the deuterium peak of D_2O at 4.6 ppm was used as a reference peak.

Asymmetric Flow Field-Flow Fractionation (AFFFF). To determine average molecular weights and the molecular weight distribution of dextran samples, we employed an AF2000 FOCUS system, (Postnova Analytics, Landsberg, Germany) equipped with a refractive index (RI) detector (PN3140, Postnova) and a multiangle (seven detectors in the range 35−145°) light scattering detector (PN3070, λ = 635 nm, Postnova). The samples (0.5 wt % in 0.01 M NaCl) were measured using a 500 μm spacer, a regenerated cellulose membrane with a cutoff of 1000 DA (Z-MEM-AQU-425N, Postnova) for dextran samples Dex3 and Dex10, a cutoff of 10 000 for dextran sample Dex40, and an injection volume of 20 μL. Constant detector flow rates of 0.3, 0.6, and 1 mL/min were used for dextran samples Dex3, Dex10, and Dex40, respectively. The focusing time was 2 min at a cross flow of 1 mL/min for Dex3 and 3 min at a cross flow of 1.1 mL/min for Dex10 and Dex40. During the elution step, the cross flow was linearly reduced to zero in 5 min for Dex3 and Dex10 but was constant for 15 min for Dex40.

Measurement of the Degree of Conjugation. The degree of lysine conjugation was measured by a trinitrobenzenesulfonic acid (TNBS) assay[38] and UV−vis spectroscopy. Briefly, 1 mL solutions of all six samples (Dex3-L1, Dex3-L2, Dex10-L1, Dex10-L2, Dex40-L1, and Dex40-L2) at a concentration of 0.1 wt % in water were prepared. To each, 1 mL of 4% (w/v) sodium bicarbonate (pH 8.5) was added, followed by the addition of 0.05% (w/v) trinitrobenzenesulfonic acid. The samples were covered with aluminum foil to protect them from light exposure, and the solutions were mixed at 40 °C in an incubator shaker for 3 h. A solution of 10% w/v sodium dodecyl sulfate (SDS) in water (1 mL) was then added, followed by slow addition of 0.5 mL of 1 M HCl. The absorbance of the samples was measured at a

https://doi.org/10.1021/acsabm.1c00544
ACS Appl. Bio Mater. 2021, 4, 6832−6842

Scheme 1. Synthesis Procedure for Lysine- and TRITC-Conjugated Dextran

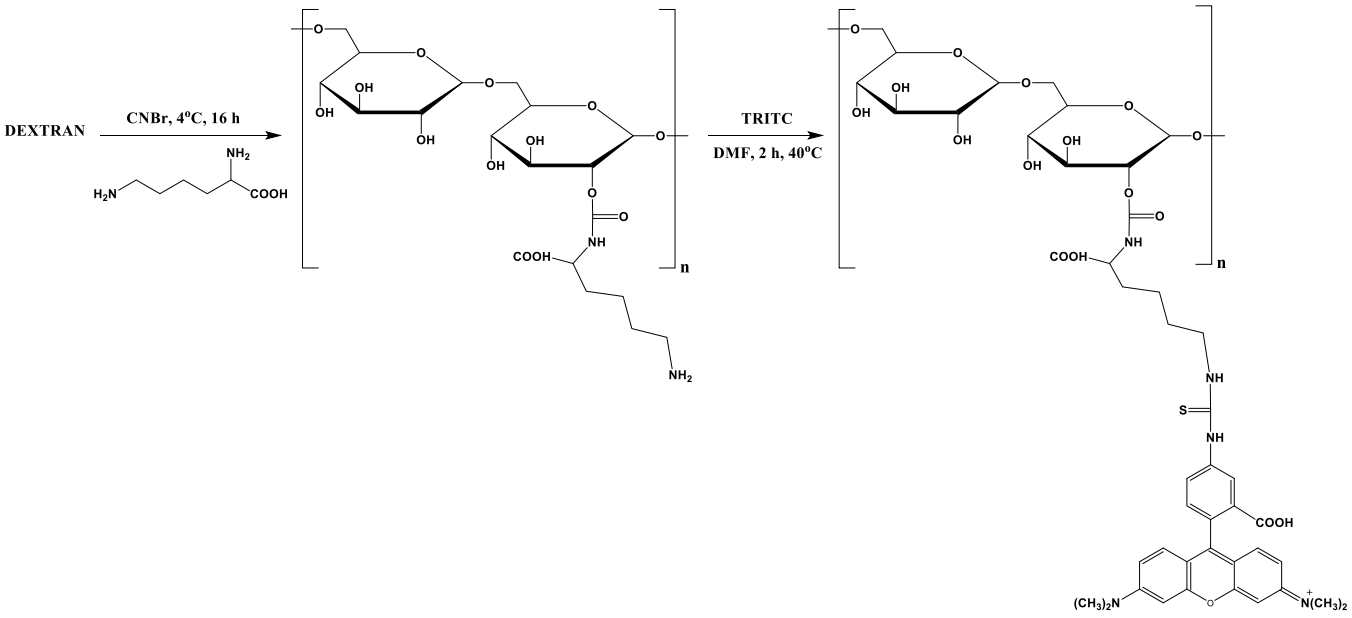

wavelength of 345 nm. To obtain a standard curve, 6-aminocaproic acid was used as an analogue for lysine. Five standard solutions of the 6-aminocaproic acid with concentrations in the range of 0.01−0.09% w/v were prepared, and the absorbance was measured at 345 nm using water as the blank sample. A linear absorbance curve at the given concentrations was obtained to calculate the molar absorbance coefficient (ε) (Figure S1). The values of unknown concentrations were calculated using the Beer−Lambert law for a quartz cuvette with a 1 cm path length.

To calculate the molar ratio of TRITC to dextran, we measured the absorbance of the samples at a wavelength of 552 nm and a polymer concentration of 0.1 wt % and the samples were dissolved in DMSO. A standard curve was obtained for five concentrations of TRITC, spanning from 0.01 to 0.05% w/v in DMSO. The value of ε was calculated in DMSO medium (Figure S2).

Dynamic Light Scattering Measurements. DLS experiments were carried out using an ALV/CGS-8F and an LS spectrometer goniometer system with a He−Ne laser operating at a wavelength of 632.8 nm and a diode-pumped solid-state laser operating at a wavelength of 660 nm. Six scattering angles in the range 39−124° were monitored simultaneously to measure the intensity autocorrelation function. The laser beam was focused on the sample cell (10 mm NMR tubes, Wilmad Glass Co., of the highest quality) through a controllable sample chamber filled with a refractive index matching liquid (*cis*-decalin) at 25 °C. The samples were dissolved in D_2O and filtered in an atmosphere of dust-free air through 0.45 μm filters directly into precleaned and dust-free 10 mm NMR tubes. From DLS, the intensity autocorrelation function $g^2(q,t)$ is linked to the theoretically amenable first-order electric field autocorrelation function $g^1(q,t)$ through the Siegert relationship[39] $g^2(q,t) = 1 + B|g^1(q,t)|^2$. Here, B ($\leq$1) is an instrumental parameter and the quantity $q = (4\pi n/\lambda)\sin(\theta/2)$ is the wave-vector, with λ, θ, and n being the wavelength of the incident light in vacuum, scattering angle, and refractive index of the medium, respectively.

In dilute solutions of lysine-conjugated dextran molecules, the entities have a tendency to form intermolecular complexes. This leads to a situation where single molecules (fast relaxation) coexist with association complexes (slow relaxation), and in this case, the decay of the correlation function can be described by the sum of two stretched exponentials

$$g^1(t) = A_f \exp[-(t/\tau_{fe})^{\gamma}] + A_s \exp[-(t/\tau_{se})^{\beta}] \quad (1)$$

with $A_f + A_s = 1$. Parameters A_f and A_s are the amplitudes for the fast and the slow relaxation times, respectively. Variables τ_{fe} and τ_{se} are the relaxation times characterizing the fast and the slow relaxation processes, respectively.

Parameters τ_{fe} and τ_{se} in eq 1 are effective relaxation times, and β ($0 < \beta \leq 1$) and γ ($0 < \gamma \leq 1$) are measures of the widths of the distributions of relaxation times. The mean relaxation times for the fast and slow modes can be expressed as

$$\tau_f = (\tau_{fe}/\gamma)\Gamma(1/\gamma) \quad (2a)$$

$$\tau_s = (\tau_{se}/\beta)\Gamma(1/\beta) \quad (2b)$$

where $\Gamma(x)$ is the γ function.

For dilute solutions of dextran conjugated with both lysine and TRITC, a single stretched exponential provides the decay of the correlation function

$$g^1(q, t) = \exp\left[-\left(\frac{t}{\tau_{se}}\right)^{\beta}\right] \quad (3)$$

Bimodal relaxation processes have previously been reported[40−42] from DLS studies on associating polymer systems of various types. In the analysis of the correlation functions by means of eqs 1 and 3, nonlinear fitting algorithms were employed to obtain best-fit values of parameters A_f, τ_{fe}, τ_{se}, γ, and β in eqs 1, 2a, and 2b and of parameter β in eq 3.

Since both the fast and the slow relaxation modes are diffusive ($1/\tau_f = Dq^2$) for the functionalized dextrans, the apparent hydrodynamic radii ($R_{h,f}$ and $R_{h,s}$) of the species can be determined via the Stokes−Einstein relation $R_h = K_B T/6\pi\eta_0 D$, where K_B is the Boltzmann constant, T is the absolute temperature, η_0 is the solvent viscosity, and D is the mutual diffusion coefficient of single molecules or intermolecular complexes. The relaxation mode described by eq 3 is also diffusive.

Small-Angle Neutron Scattering Measurements. Neutron scattering measurements were performed using a SANS instrument with a JEEP II reactor at the Institute for Energy and Technology (IFE) at Kjeller (Norway). A velocity selector (Dornier) was used with a wavelength spread of $\Delta\lambda/\lambda$ = 10%. Two different sample detector distances (1.0 and 3.4 m) and two different neutron wavelengths (5.1 and 10.2 Å) were used to obtain a total scattering range (q-range) from 0.008 to 0.32 Å^{-1}, corresponding to an observable particle size range of approximately 2−80 nm. The

https://doi.org/10.1021/acsabm.1c00544
ACS Appl. Bio Mater. 2021, 4, 6832−6842

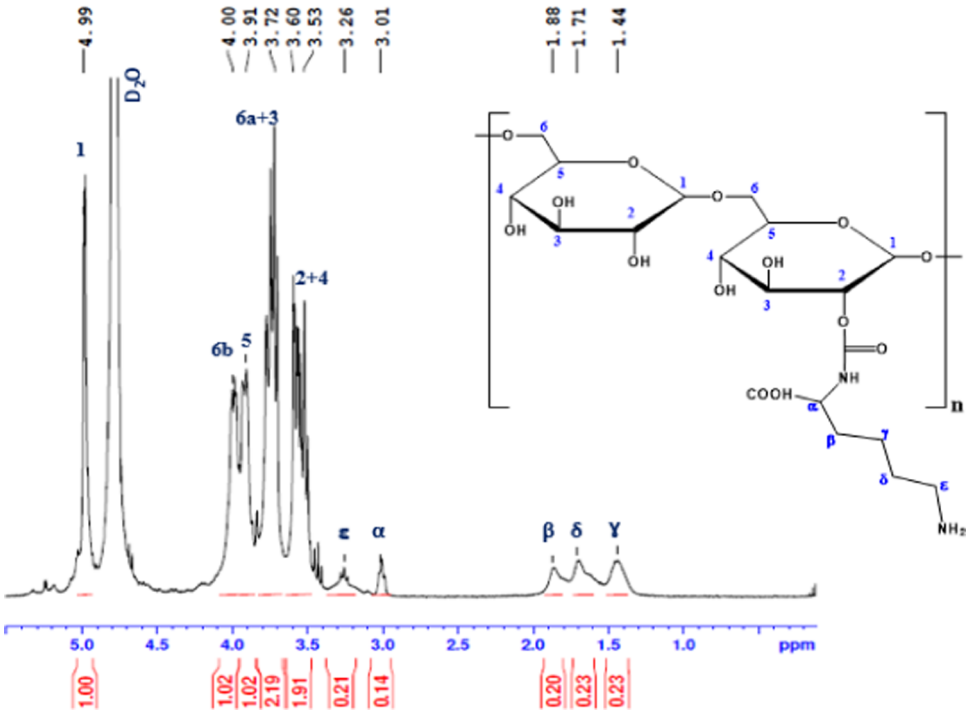

Figure 1. Typical ^{1}H NMR spectrum of lysine-conjugated dextran (sample Dex3-L2, Table 1).

neutron detector was a circular ^{3}He-filled RISØ type placed inside a shielded detector chamber with vacuum to reduce air scattering. All samples were dissolved in D_2O to reduce incoherent scattering and to maximize the scattering contrast. The samples were introduced into 5 mm quartz cuvettes and placed in a temperature-controlled sample chamber. All measurements were performed at 25 °C. The transmission was measured separately, and the scattering was normalized to absolute units (cm^{-1}) by taking into account data from an empty cell, beam without cell, and blocked-beam background scattering for data reduction.

Axonal Tracing, Tissue Clearing, and Laser Scanning Confocal Microscopy. Lumbar spinal cords of chicken embryos at 10−11 days of incubation were dissected out in the ice-cold chicken Ringer solution (containing, in mM, NaCl 137, KCl 5, $CaCl_2$ 2, $MgCl_2$ 1, $NaPO_4$ 1, HEPES 5, and D-glucose 11, pH 7.4) bubbled with 100% O_2. They were then labeled with the Dex3-L2-R, Dex10-L2-R, and Dex40-L2-R samples using the technique of Glover et al.[36]

Briefly, a small amount of each conjugated dextran sample was dissolved in a 0.5 μL drop of distilled water until the solution reached a viscosity high enough to facilitate the collection of small globules of tracer onto the tips of fine, sharpened stainless steel needles, where they dried to form solid crystals. A transverse cut was made unilaterally across the dorsal surface of the lumbar spinal cord to sever axons in the dorsal columns, and several conjugated dextran crystals were inserted into the cut sequentially, each being allowed to dissolve and remain for about 30 s before applying the next. This was continued for 3−4 min to allow uptake of the conjugated dextrans into the cut axons.

To directly compare the efficiency of labeling, two different conjugated dextran samples were applied on the left and right sides of each spinal cord, respectively. Spinal cords labeled with Dex3-L2-R versus Dex10-L2-R were incubated for either 3 or 7 h, whereas spinal cords labeled with Dex10-L2-R versus Dex40-L2-R were incubated for 7 h in continuously oxygenated chicken Ringer at ambient temperature (24 °C).

Following incubation, the labeled spinal cords were briefly inspected under a fluorescence microscope and then fixed with 4% paraformaldehyde in phosphate-buffered saline (pH 7.4). The tissue was then cleared using the uDISCO procedure.[43]

To visualize fine details of the retrograde and anterograde labeling, *Z*-stacks of confocal images of all cleared spinal cords were obtained using a Zeiss LSM700 microscope with a 10× objective (NA = 0.25). For presentation here, each *Z*-stack was flattened into a composite *Z*-axis projection using the SUM Slide command in ImageJ.

RESULTS AND DISCUSSION

^{1}H NMR Spectroscopy. Six samples with different degrees of lysine conjugation were prepared. The degree of lysine conjugation was tuned by the amount of cyanogen bromide and lysine in the solution. ^{1}H NMR (Bruker 400 MHz, D_2O, δ, ppm) spectra of lysine-conjugated dextran in D_2O exhibited the characteristic signal of protons from lysine (Figure 1). We attribute the peaks in the range 3.4−5 ppm to the anomeric and ring protons of dextran: δ = 4.99 (1H, d, J = 3.1 Hz, H-1), 4.00 (1H, d, J = 7.5 Hz, H-6a or H-6b), 3.91 (1H, d, J = 9.0 Hz, H-5), 3.76 (1H, d, J = 10.5 Hz, H-6a or H-6b), 3.72 (1H, app.t, J = 9.3 Hz, H-3), 3.60 (1H, dd, J = 6.3, 3.4 Hz, H-2), 3.53 (1H, t, J = 9.3 Hz, H-4). However, the low-signal-intensity peaks in the range 1.4−3.3 ppm represent lysine monomers conjugated to the dextran backbone. The chemical shift values of the signals in ^{1}H NMR spectra of the dextran and lysine moiety of this product were in accordance with literature values.[44−46] The degree of substitution (DS) of lysine per each glucose unit was calculated by dividing the integral of the peak at 3.01 ppm, corresponding to 1 proton of lysine, with that of the peak at 4.99 ppm, corresponding to 1 proton from a single unit of glucose. DS ranged between 0.05 and 0.06 for the samples labeled as L1 and from 0.08 to 0.14 for the samples labeled as L2. In terms of percentage, it was calculated to be 1.7−2 and 2.7−4.6% for the samples labeled as L1 and L2, respectively.

The hydroxyl groups of dextran combine with cyanogen bromide to give the reactive cyclic imidocarbonate. The activated dextran then reacts with the α-amino group of lysine under mild basic conditions, thus generating an iso-urea

https://doi.org/10.1021/acsabm.1c00544
ACS Appl. Bio Mater. 2021, 4, 6832−6842

linkage. Adjusting pH to 8.4 favors the activity of the α-amino group, rather than ε-amines, and this provides enough free amine groups on the backbone for further reactions with TRITC.

Degree of Conjugation of Lysine and TRITC. To calculate the mol ratio of lysine and TRITC using the TNBS assay, we needed the number average molecular weights (M_n) of the dextran samples with weight-average molecular weights (M_w) of 3500 and 10 000. Measurements were performed using an AFFFF instrument and processed with Postnova software (AF2000 Control, version 1.1.011) using a Zimm-type fit. As an example, the molecular weight and dispersity index (M_w/M_n) of the Dex3 sample are shown in Figure 2.

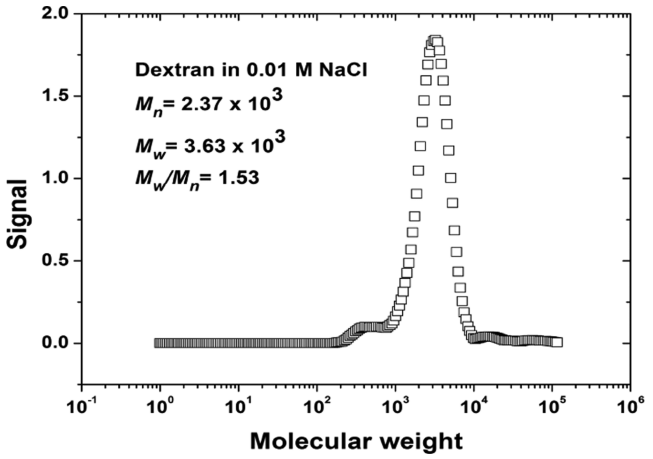

Figure 2. Typical illustration of the molecular weight distribution of Dex3 in 0.5 wt % in 0.01 M NaCl, obtained with the AFFFF instrument.

Measuring the free amine groups by the TNBS assay revealed that increasing the feed ratio of lysine and cyanogen bromide by a factor of 2 resulted in a substantial (1.6−2.2 fold) increase in the amount of lysine conjugated to dextran (compare L2 to L1 samples in Table 2). To assess the degree

Table 2. Degree of Lysine and TRITC Conjugation[a]

sample	mol lysine per mol dextran	sample	mol TRITC per mol dextran	percentage of amino groups used by TRITC
Dex3-L1	0.54	Dex3-L1-R	0.25	0.46
Dex3-L2	1.18	Dex3-L2-R	0.50	0.42
Dex10-L1	2.87	Dex10-L1-R	1.30	0.45
Dex10-L2	4.75	Dex10-L2-R	1.97	0.41
Dex40-L1	9.73	Dex40-L1-R	4.40	0.45
Dex40-L2	15.12	Dex40-L2-R	7.27	0.48

[a]The errors in the values given in the table are less than 5%.

of TRITC conjugation, we assessed absorbance at 552 nm, the maximum absorbance wavelength for the dye in DMSO. Figure 3 shows the UV−vis spectrum of the Dex3-L2-R sample with the absorbance peak of trinitrophenyl (TNP)-labeled amino groups of lysine at 352 nm and the absorbance peak of TRITC at 557 nm in distilled water.

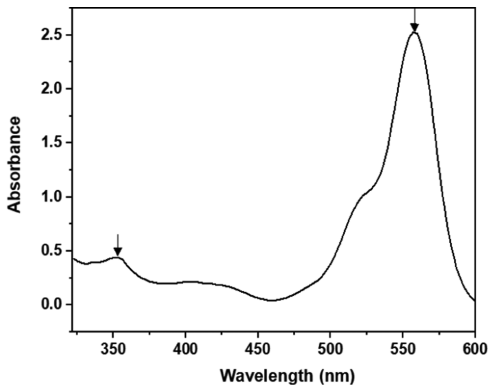

Figure 3. Vis−UV spectrum of Dex3-L2-R (0.1 wt %) demonstrating the conjugation of lysine and TRITC with the absorbance peaks of 352 and 557 nm in distilled water.

TRITC has an isothiocyanate reactive group (−N═C═S), which is an amine-reactive group and reacts with the primary amine groups on lysine. Keeping the value of pH around 8.4 during the lysine−dextran synthesis favors the reactivity of the α-amino groups of lysine; this leaves the ε amine groups on the backbone of lysine free to react with TRITC. As an amine-reactive derivative of rhodamine, TRITC will react with available amine groups provided by the lysine moieties, and as expected, its degree of conjugation paralleled that of lysine (Table 2).

Dynamic Light Scattering. The correlation function data at the indicated scattering angles for 0.1 wt % solutions of the lysine- and TRITC-conjugated dextrans in D_2O at 25 °C is shown in Figure 4. DLS results showed that the normalized correlation functions for the lysine-conjugated samples (without TRITC) can be described by two stretched exponential relaxation modes. The fast relaxation mode yielded values of hydrodynamic radius ($R_{h,f}$) of 1.73 ± 0.07, 3.0 ± 0.1, and 5.1 ± 0.2 nm for Dex3, Dex10, and Dex40 samples, respectively. We ascribe these values to molecularly dispersed unconjugated dextran entities (Figure 5a, red bars), as they are in accordance with previous findings of unconjugated dextrans of the same molecular weights.[47−49] We measured the hydrodynamic radii of unreacted dextrans as 1.9, 3.3, and 5.6 nm for weight-average molecular weights (M_w) of 3500, 10 000, and 40 000, respectively.

We ascribe the larger species (Figure 5a, blue bars) to lysine-conjugated dextrans (without TRITC conjugation), which have likely formed intra- and intermolecular hydrogen bonds between the amine groups of lysine and hydroxyl groups in dextran.[24,50,51] The fact that the hydrodynamic radius is as large as 100 nm suggests the formation of intermolecular association complexes. We note that the sizes of the individual molecules of the dextrans (as given above) are much smaller than the corresponding association complexes, suggesting that these aggregates all contain a large number of molecules. Under these conditions, the size of a complex is not expected to be directly related to the size of an individual molecule but instead to the manner in which these molecules interact, and consequently, to how many molecules accumulate into one complex. The balance between enthalpic and entropic contributions, along with steric hindrances, governs this situation. We do not have information to determine this "aggregation number" independently. However, it is highly likely that the branching present in Dex40 strongly affects this

https://doi.org/10.1021/acsabm.1c00544
ACS Appl. Bio Mater. 2021, 4, 6832−6842

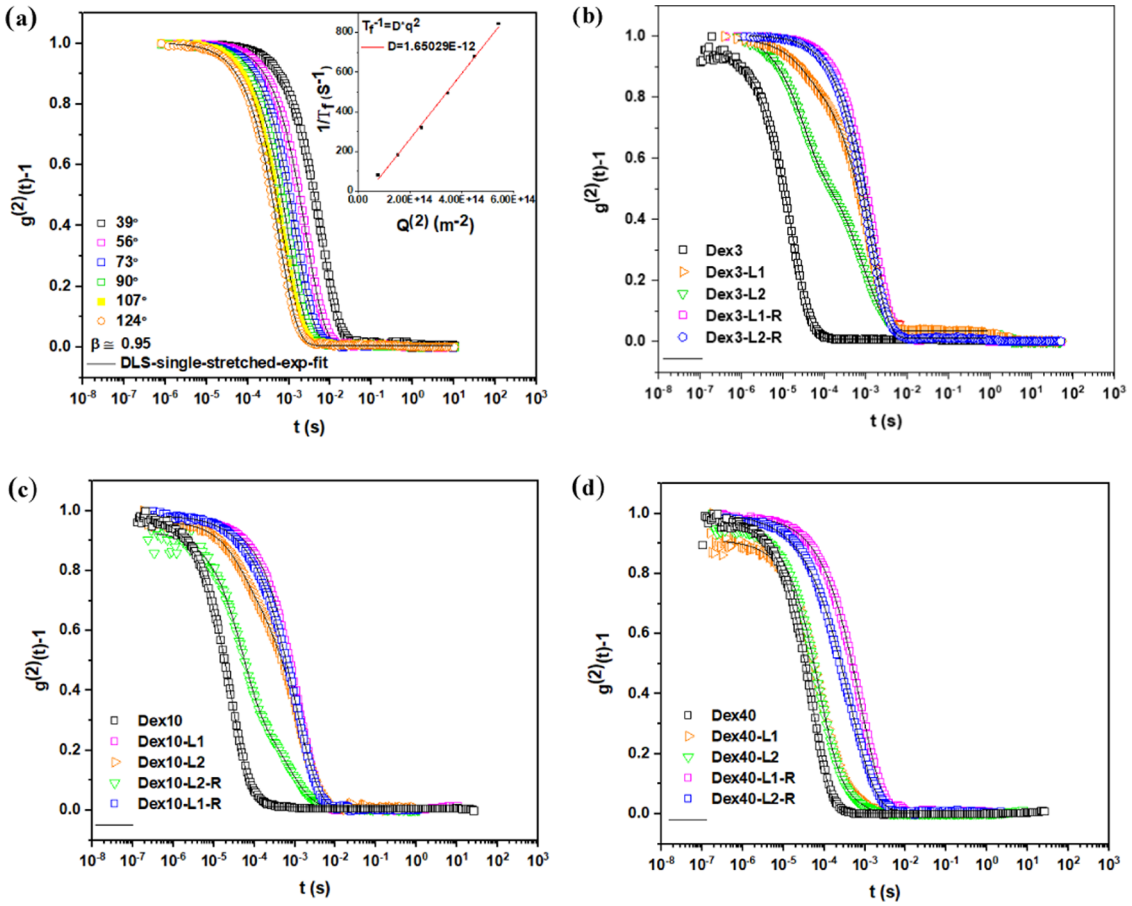

Figure 4. First-order electric field autocorrelation functions versus time and their corresponding fitted curves for sample Dex3-L1-R at the indicated scattering angles (a) and for the indicated dextran samples of M_w = 3500 (b), M_w = 10 000 (c), and M_w = 40 000 (d) at a scattering angle of 73°.

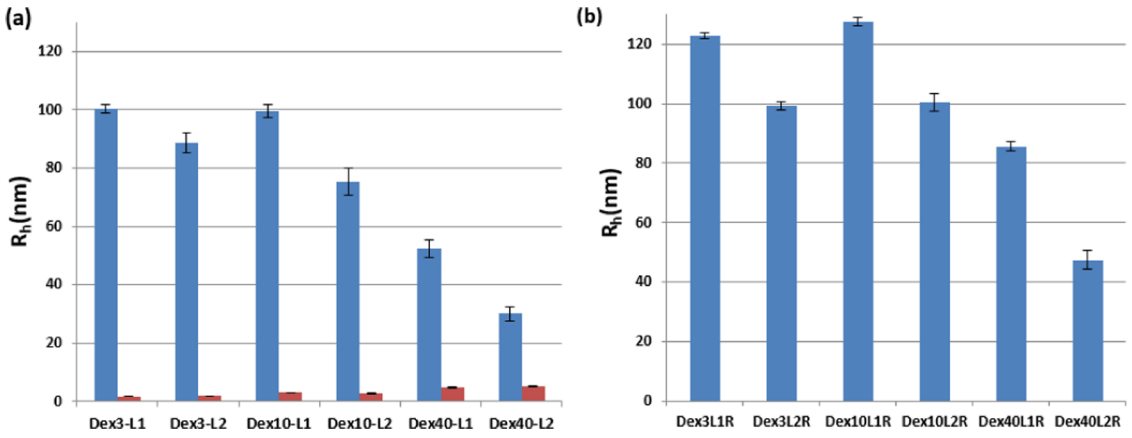

Figure 5. Hydrodynamic radii for (a) lysine-conjugated and (b) lysine- and TRITC-conjugated dextran samples. The polymer concentration is 0.1 wt % for all samples. The red bars represent the hydrodynamic radii determined from the fast relaxation mode. The blue bars represent the hydrodynamic radii calculated from the slow relaxation mode, and on the top, the error bars are indicated.

balance, resulting in smaller complexes due to fewer associating molecules, tighter bonding, or a combination of these effects. It is evident from Figure 5a that we have the smallest values of the hydrodynamic radius for the Dex40−lysine complexes. From light scattering studies[47] on dextrans of various molecular weights, it was concluded that short dextran chains do not contain branching points, whereas dextrans with molecular weights of 40 000 and above are branched and exhibit a hyperbranched structure. The conjecture is that in this case, we obtain compact entities with fewer associating units. It has been reported that Dex40 contains about 4% branching,[52] which corresponds to approximately four branching points per chain.[53] It has been argued that for molecular weights of 10 000 and lower, no branching points are detected in dextrans.[54]

A general feature seen in Figure 5a for the dextran−lysine complexes is that R_h values are lower when the degree of lysine conjugation is increased. This is a systematic trend observed for all molecular weight samples, and this finding may be rationalized in the following way. When the degree of lysine

https://doi.org/10.1021/acsabm.1c00544
ACS Appl. Bio Mater. 2021, 4, 6832−6842

Scheme 2. Suggested Scheme for Intermolecular Hydrogen-Bonding and Hydrophobic Interactions in Conjugated Dextran Chains[a]

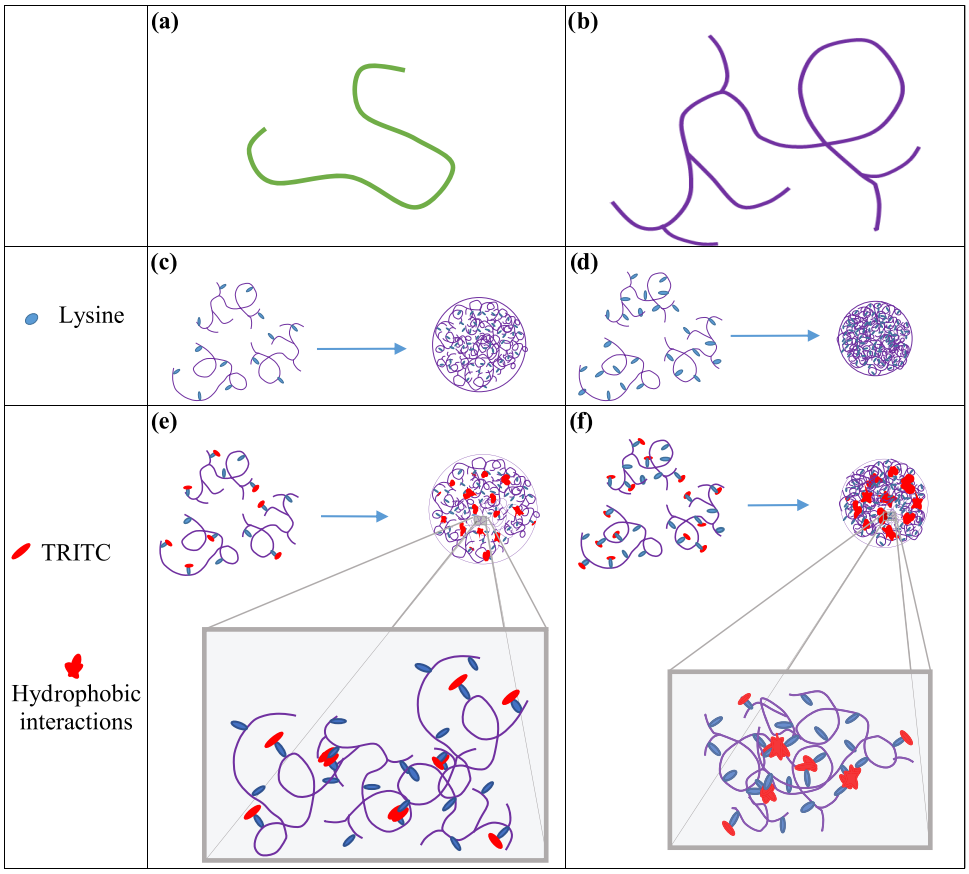

[a]a) Illustration of low-molecular-weight dextran with a linear structure and (b) high-molecular-weight dextran chain with a branched structure. (c) Lysine-conjugated dextrans (Dex40-L1). Inter- and intramolecular hydrogen bonds form between the amine groups of lysine and the hydroxyl groups of dextran. (d) Increasing the lysine conjugation by a factor of 2 (Dex40-L2) hampers the process of forming aggregates, causing smaller-sized conjugates. (e) Lysine- and TRITC-conjugated dextrans. (f) Intramolecular hydrophobic interactions are greater when the TRITC conjugation is doubled as a result of the doubling of lysine conjugation (Dex40-L2-R), causing greater contraction and smaller size compared to Dex40-L1-R, in which intermolecular hydrophobic interactions are more dominant.

conjugation increases, the dextran entities are equipped with more lysine groups; this increases the charge density of the dextran moieties and makes the dextran molecules more hydrophilic. As a result, the conjugated dextran molecules are less disposed to form aggregates and this explains the smaller size of the conjugates. Interactions through hydrogen bonds may also come into play and affect the size of the conjugates. It is known that hydrogen bonds can play a fundamental role for interactions in aqueous dextran solutions, even be a dominant actor in the crystallization process in concentrated aqueous solutions of low-molecular-weight dextrans.[53]

By contrast to lysine-conjugated samples (without TRITC), where we observed two relaxation modes, the normalized correlation functions for the lysine- and TRITC-conjugated samples could be described well by a single stretched exponential (Figure 5b). The hydrophobic feature of the TRITC component (cf. Scheme 1) portends additional hydrophobic interactions, and this may lead to enhanced aggregation. The general trend is the same as in Figure 5a, but Figure 5b shows that the values of the hydrodynamic radii for the dextran−lysine−TRITC conjugates are significantly larger than the corresponding values for the dextran−lysine samples. In this case, we surmise that additional intermolecular hydrophobic interactions provided by TRITC lead to the formation of larger species (Figure 5b) and that most of the single dextran entities are assimilated in this process, so the fast relaxation mode disappears.

We present a plausible scheme for hydrogen-bonding and hydrophobic interactions within and between conjugated dextran chains in Scheme 2. Two different illustrations of lower molecular weight and higher molecular weight of dextran are shown in Scheme 2a,b, respectively. We elucidate a dextran of a molecular weight of 40 000 with a branched structure (Scheme 2b) and Dex3 and Dex10 with linear structures (Scheme 2a). To explain the intra- and intermolecular interactions after lysine and TRITC conjugation, we demonstrate the addition of different amounts of lysine to Dex40 as an example (Scheme 2c,d). Hydrogen bonds can form between the amine groups of lysine and the hydroxyl groups of dextran after conjugation of lysine to the dextran backbone (Scheme 2c). Increasing the lysine conjugation by a factor of 2 (Dex40-L2) makes the conjugate species more hydrophilic and provides them with a higher charge density, this reduces the tendency of the moieties to form aggregates, and we expect conjugates of smaller sizes (Scheme 2d). Hydrogen bonds are probably important for the interactions.

https://doi.org/10.1021/acsabm.1c00544
ACS Appl. Bio Mater. 2021, 4, 6832−6842

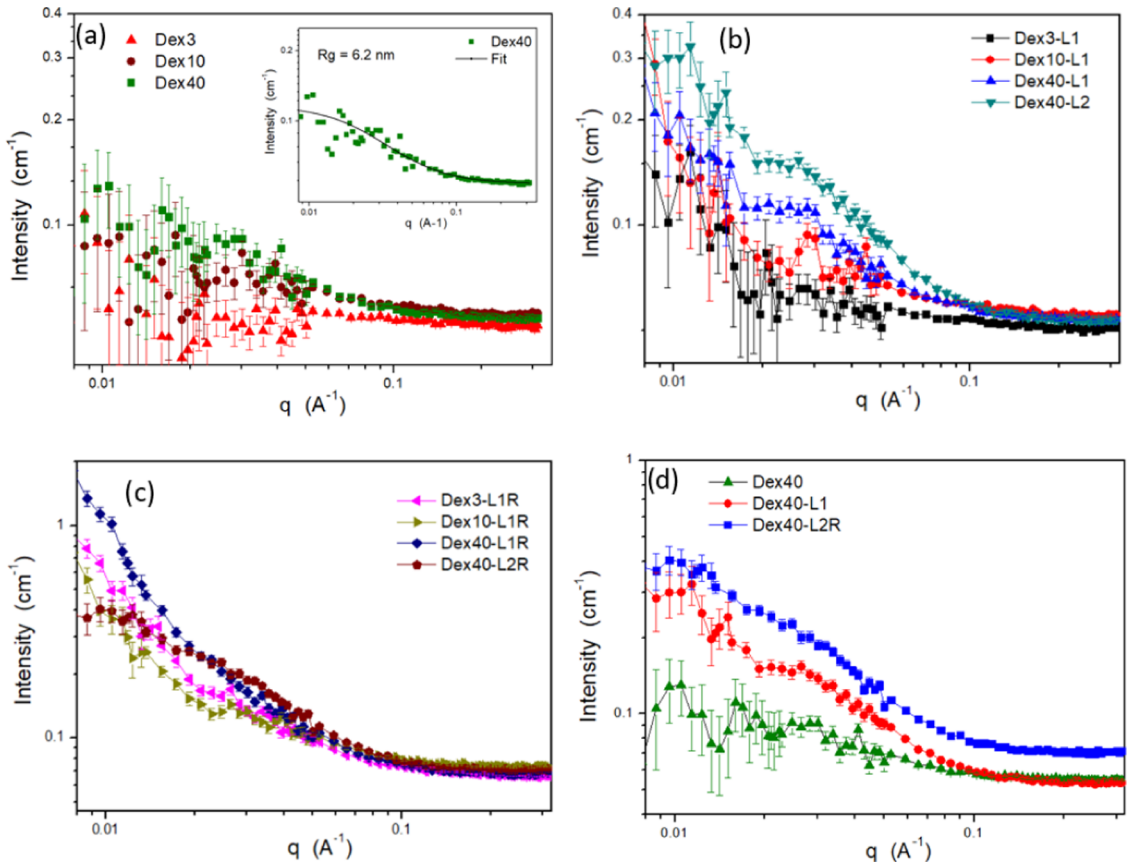

Figure 6. (a) SANS data for 1 wt % samples of unconjugated dextrans of different molecular weights (Dex3, Dex10, and Dex40). The inset shows fitting of Dex40 results with a Gaussian coil model, (b) SANS data for 1 wt % lysine-conjugated dextran samples, (c) SANS data for 1 wt % lysine- and TRITC-conjugated dextran samples, (d) comparison plot to highlight differences between 40 000 molecular weight dextrans with and without conjugation.

Attaching TRITC to lysine-conjugated dextran introduces intra- and intermolecular hydrophobic interactions (Scheme 2e). Effects of hydrophobic interactions from TRITC on the Dex40 conjugates are illustrated in Scheme 2f.

Small-Angle Neutron Scattering. SANS is a powerful technique to probe structures on a mesoscopic scale. SANS in 1 wt % solutions of unconjugated dextran of different molecular weights is displayed in Figure 6a. The scattering was very weak, and there were no significant differences in the scattering pattern between the three different molecular weights. This suggests the presence of highly hydrated, low-density structures with little local contrast to the surroundings. However, for the highest molecular weight (M_w = 40 000), it was possible to discern the typical profile of a coil in the solution; the scattering data could be fitted with the aid of a Gaussian coil model for this sample (see the inset in Figure 6a). If we assume a dispersity index (M_w/M_n) of 1.5, this yields a radius of gyration R_g = 6.2 nm. From DLS, we determined a value of R_h = 5.1 ± 0.2 nm, which is very close to a previously reported value[49] of 4.9 nm for the same molecular weight dextran. The structure-sensitive dimensionless ratio[55] $\rho = R_g/R_h$ then yields a value of ρ = 1.2, which is close to the 1.225 value that was theoretically predicted[56] for hyperbranched structures on the basis of the Kirkwood−Riseman preaverage approximation.[57] This result therefore indicates a highly branched structure for M_w = 40 000 dextran.[52]

Figure 6b shows SANS scattering results for lysine-conjugated dextrans of different molecular weights. The scattering intensity is now generally stronger, indicating densification of the scattering entities, in line with the illustration in Scheme 2. Close inspection reveals a weak correlation peak, located at approximately q = 0.03 Å^{-1}, which corresponds to entities with an interaction distance of about d = 21 nm ($d = 2\pi/0.03$ Å^{-1}). This correlation peak appears to be strengthened for the 40 000 M_w dextran, and an increase in the degree of lysine conjugation (Dex40-L2) appears to further promote the effect. This suggests that the correlation peak may reflect electrostatic interactions.[58] The scattering intensity does not show any signs of a plateau in the low-q region characteristic for small-sized particles, but instead a steady rise for low q values (left part of the graph). This divulges the existence of large clusters (outside the window accessible with SANS), as we reported from the slow mode in DLS. Figure 6c shows SANS scattering results for lysine- and TRITC-conjugated dextrans of different molecular weights. In this case, the scattering is even stronger (note the different vertical scales), which is a clear sign that the entities have become more compact, with a corresponding enhanced scattering contrast. The increase in the scattering intensity for low q values is also present here, demonstrating the presence of structures above the size limit of SANS (here ca. 50 nm). Note, however, that for high-molecular-weight sample Dex40-L2R a plateau has developed, demonstrating the small size of the structures formed in this case, in good accordance with the results from DLS (cf. Figure 5).

https://doi.org/10.1021/acsabm.1c00544
ACS Appl. Bio Mater. 2021, 4, 6832−6842

Figure 6d highlights the differences in SANS between unconjugated and conjugated 40 000 molecular weight dextrans. The addition of TRITC clearly changes the scattering pattern. The intensity becomes stronger at low q values, and this additional scattering obscures the correlation peak. We attribute the extra scattering to hydrophobic interactions and corresponding densification mediated by the TRITC groups (cf. Scheme 2). The addition of TRITC was also accompanied by an increase of scattering at high q values, which represents the incoherent scattering mainly due to hydrogen atoms in TRITC.

Intra-axonal Mobility. To test intra-axonal mobility, we applied lysine- and TRITC-conjugated dextrans of different molecular weights to unilateral cuts in the dorsal columns of the lumbar spinal cord, which carry sensory axons ascending to the brain, of day 10−11 chicken embryos. This leads to retrograde and anterograde labeling of the cut axons.[35,36] To compare mobilities directly, different molecular weight dextran conjugates were applied to opposite sides of each spinal cord. The fluorescence signal intensity and distance from the application site followed the order Dex3-L2-R > Dex10-L2-R ≫ Dex40-L2-R (Figure 7). Dex3-L2-R and Dex10-L2-R both labeled many hundreds of axons as well as collateral branches extending laterally from the main axons (Figure 7A−C), whereas Dex40-L2-R labeled only a handful of axons and to much shorter distances, even with longer incubation times (Figure 7C). The maximum labeling distance was consistently shorter, and the labeling intensity at any given distance was consistently lower for axons labeled with Dex10-L2-R compared to Dex3-L2-R.

We and others have reported previously that 3 kD conjugated dextrans are more efficient for retrograde and anterograde axonal tracing than 10 kD conjugated dextrans, traveling both faster and farther.[35,37,59] The mechanism of intra-axonal mobility is not known; however, Fritzsch[59] showed that intra-axonal mobility of conjugated dextrans is not affected by disruption of microtubules, indicating that it is independent of microtubule-based active axonal transport. Given that the volume of conjugated dextran particles decreases with the molecular weight, the greater mobility of Dex3-L2-R seems to conflict with a pure diffusion mechanism since it does not accord with the inverse relationship between diffusion rate and particle size. However, the intra-axonal mobility of conjugated dextrans may be affected by several factors, such as the concentration of the conjugates in the tissue, interactions between the conjugated dextrans and the intra-axonal molecular milieu, possible confinements and shear forces in the transport process, and the size and structure of the conjugates. We suggest therefore that the differences in mobilities of 3 and 10 kD conjugated dextran can be attributed to these factors.

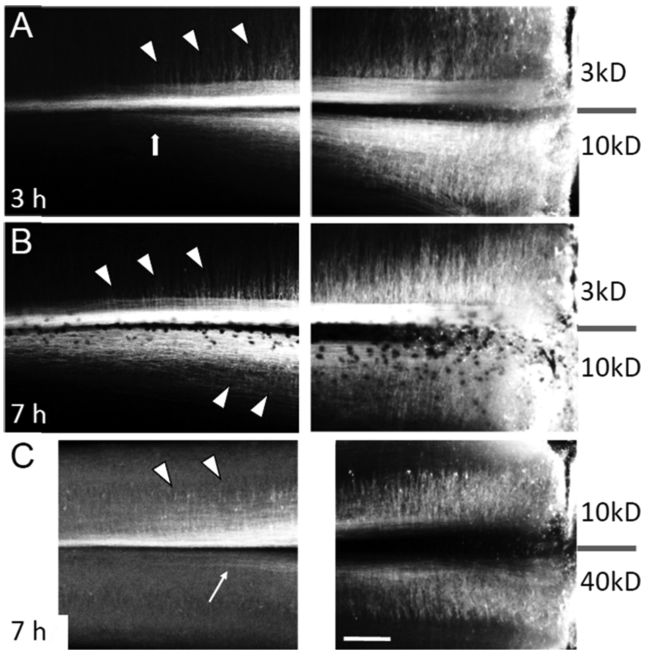

Figure 7. Intra-axonal mobility of lysine- and TRITC-conjugated dextrans of different molecular weights. Each panel is a projection of a confocal Z-stack. Right panels are taken just rostral to the dextran application sites (which are visible at the right edge of the panel), left panels are centered about 5 spinal segments more rostral. The black bars to the right indicate the midline, on either side of which the indicated molecular weight dextrans were applied to the dorsal columns, thus anterogradely labeling sensory axons ascending toward the brain (these axons were also retrogradely labeled back to the sensory neuron somata, not shown). Incubation times are as indicated in the left panels. The 3 and 10 kD dextrans consistently labeled large numbers (many hundreds) of axons, including collateral branches extending laterally from the main axon tract (carats in A, B, and C), whereas 40 kD dextran labeled only a handful of axons (small arrow in C). The vertical arrow in (A) shows the rostral limit of labeling by 10 kD dextran at 3 h. The labeling distance attained by 10 kD dextran increased after an additional 4 h of incubation (B), but the labeling intensity at any given distance was substantially lower than that for 3 kD dextran. The scale bar is 100 μm.

CONCLUSIONS

We prepared different molecular weight dextrans with different degrees of conjugation with lysine and TRITC. DLS and SANS analyses showed that lysine-conjugated dextrans form association complexes, probably through intermolecular hydrogen-bonding interactions, and that the volume of association complexes decreases with an increasing degree of conjugation. We propose that the more the lysine conjugated to the dextran backbone, the more the intramolecular interactions outcompete intermolecular interactions and the smaller the volume. All three molecular weight dextrans exhibited this pattern, but the effect also increased with increasing molecular weight, probably because of the higher degree of branching at higher molecular weights, providing greater opportunity for intramolecular interactions. The volume of association complexes increased with the addition of TRITC, probably due to hydrophobic interactions. However, increasing the degree of TRITC conjugation increased compaction again, probably due to an increase in intramolecular hydrophobic interactions.

Intra-axonal mobility is inversely proportional to molecular weight as previously reported, but this unexpectedly means that the larger the molecular volume, the higher the mobility. Intra-axonal mobility of the conjugated dextran association complexes is not due to simple diffusion. Since earlier studies rule out a microtubule-mediated axonal transport mechanism, the mobility must involve other molecular interactions within the intracellular milieu.

These data provide information that is important for developing dextran nanoparticles as intra-axonal biomolecule carrier systems for research and clinical applications.

https://doi.org/10.1021/acsabm.1c00544
ACS Appl. Bio Mater. 2021, 4, 6832−6842

■ ASSOCIATED CONTENT

Supporting Information

The Supporting Information is available free of charge at https://pubs.acs.org/doi/10.1021/acsabm.1c00544.

Standard absorbance curves and calculation of the extinction coefficient (PDF)

■ AUTHOR INFORMATION

Corresponding Authors

Joel C. Glover − *Laboratory of Neural Development and Optical Recording (NDEVOR), Department of Molecular Medicine, Institute of Basic Medical Sciences, University of Oslo, Oslo N-0317, Norway; Norwegian Center for Stem Cell Research, Oslo University Hospital, Oslo N-0317, Norway*; Email: joel.glover@medisin.uio.no

Bo Nyström − *Department of Chemistry, University of Oslo, Oslo N-0315, Norway*; orcid.org/0000-0002-6903-4423; Email: b.o.g.nystrom@kjemi.uio.no

Authors

Darya Zeini − *Department of Chemistry, University of Oslo, Oslo N-0315, Norway; Laboratory of Neural Development and Optical Recording (NDEVOR), Department of Molecular Medicine, Institute of Basic Medical Sciences, University of Oslo, Oslo N-0317, Norway*

Kenneth D. Knudsen − *Institute for Energy Technology, Kjeller N-2027, Norway*

Complete contact information is available at: https://pubs.acs.org/10.1021/acsabm.1c00544

Author Contributions

The manuscript was written through the contribution of all authors. All authors have given approval to the final version of the manuscript.

Funding

This research was funded by the University of Oslo Life Science Program and private donations from the Norwegian ALS patient advocacy group ALS-Norge.

Notes

The authors declare no competing financial interest.

■ ACKNOWLEDGMENTS

The authors acknowledge technical assistance from Kobra Sultani at NDEVOR. The authors appreciate the valuable help that they received from Vahid Forooqi Motlaq and Dr. Kaizheng Zhu in measuring and analyzing the A4F data and Prof. Trond Vidar Hansen for helping them in the interpretation of NMR spectra.

■ REFERENCES

(1) Wang, H.; Dai, T.; Zhou, S.; Huang, X.; Li, S.; Sun, K.; Zhou, G.; Dou, H. Self-assembly assisted fabrication of dextran-based nanohydrogels with reduction-cleavable junctions for applications as efficient drug delivery systems. *Sci. Rep.* **2017**, *7*, No. 40011.

(2) Zink, M.; Hotzel, K.; Schubert, U. S.; Heinze, T.; Fischer, D. Amino Acid−Substituted Dextran-Based Non-Viral Vectors for Gene Delivery. *Macromol. Biosci.* **2019**, *19*, No. 1900085.

(3) Qu, J.; Liang, Y.; Shi, M.; Guo, B.; Gao, Y.; Yin, Z. Biocompatible conductive hydrogels based on dextran and aniline trimer as electro-responsive drug delivery system for localized drug release. *Int. J. Biol. Macromol.* **2019**, *140*, 255−264.

(4) Zhang, M.; Liu, J.; Kuang, Y.; Li, Q.; Zheng, D.-W.; Song, Q.; Chen, H.; Chen, X.; Xu, Y.; Li, C.; et al. Ingenious pH-sensitive dextran/mesoporous silica nanoparticles based drug delivery systems for controlled intracellular drug release. *Int. J. Biol. Macromol.* **2017**, *98*, 691−700.

(5) Prusty, K.; Swain, S. K. Nano silver decorated polyacrylamide/dextran nanohydrogels hybrid composites for drug delivery applications. *Mater. Sci. Eng. C* **2018**, *85*, 130−141.

(6) Jamwal, S.; Ram, B.; Ranote, S.; Dharela, R.; Chauhan, G. S. New glucose oxidase-immobilized stimuli-responsive dextran nanoparticles for insulin delivery. *Int. J. Biol. Macromol.* **2019**, *123*, 968−978.

(7) Joshy, K.; George, A.; Snigdha, S.; Joseph, B.; Kalarikkal, N.; Pothen, L. A.; Thomas, S. Novel core-shell dextran hybrid nanosystem for anti-viral drug delivery. *Mater. Sci. Eng. C* **2018**, *93*, 864−872.

(8) Li, C.; Wang, J.; Wang, Y.; Gao, H.; Wei, G.; Huang, Y.; Yu, H.; Gan, Y.; Wang, Y.; Mei, L.; et al. Recent progress in drug delivery. *Acta Pharm. Sin. B* **2019**, *9*, 1145−1162.

(9) Varshosaz, J. Dextran conjugates in drug delivery. *Expert Opin. Drug Delivery* **2012**, *9*, 509−523.

(10) Huang, S.; Huang, G. Preparation and drug delivery of dextran-drug complex. *Drug Delivery* **2019**, *26*, 252−261.

(11) Sur, S.; Rathore, A.; Dave, V.; Reddy, K. R.; Chouhan, R. S.; Sadhu, V. Recent developments in functionalized polymer nanoparticles for efficient drug delivery system. *Nano-Struct. Nano-Objects* **2019**, *20*, No. 100397.

(12) Ingusci, S.; Verlengia, G.; Soukupova, M.; Zucchini, S.; Simonato, M. Gene therapy tools for brain diseases. *Front. Pharmacol.* **2019**, *10*, No. 724.

(13) Huang, G.; Huang, H. Application of dextran as nanoscale drug carriers. *Nanomedicine* **2018**, *13*, 3149−3158.

(14) Jeong, M.; Kim, Y.; Kim, J.; Ferrante, D. D.; Mitra, P. P.; Osten, P.; Kim, D. Comparative three-dimensional connectome map of motor cortical projections in the mouse brain. *Sci. Rep.* **2016**, *6*, No. 20072.

(15) Miranda-Vilela, A. L.; Peixoto, R. C. A.; Longo, J. P. F.; Portilho, F. A.; Miranda, K. L. C.; Sartoratto, P. P. C.; Báo, S. N.; de Azevedo, R. B.; Lacava, Z. G. M.; et al. Dextran-functionalized magnetic fluid mediating magnetohyperthermia combined with preventive antioxidant pequi-oil supplementation: potential use against cancer. *J. Biomed. Nanotechnol.* **2013**, *9*, 1261−1271.

(16) Togami, W.; Sei, A.; Okada, T.; Taniwaki, T.; Fujimoto, T.; Tahata, S.; Nagamura, K.; Nakanishi, Y.; Mizuta, H. Effects of the water-holding capability of polyvinyl formal sponges on osteogenic ability in in vivo experiments. *J. Biomed. Mater. Res., Part B* **2015**, *103*, 188−194.

(17) Huang, H.; Liu, M.; Luo, S.; Wang, K.; Wan, Q.; Deng, F.; Xu, D.; Zhang, X.; Wei, Y. One-step preparation of AIE-active dextran via formation of phenyl borate and their bioimaging application. *Chem. Eng. J.* **2016**, *304*, 149−155.

(18) Xie, M.; Lei, H.; Zhang, Y.; Xu, Y.; Shen, S.; Ge, Y.; Li, H.; Xie, J. Non-covalent modification of graphene oxide nanocomposites with chitosan/dextran and its application in drug delivery. *RSC Adv.* **2016**, *6*, 9328−9337.

(19) Lee, S.; Stubelius, A.; Hamelmann, N.; Tran, V.; Almutairi, A. Inflammation-responsive drug-conjugated dextran nanoparticles enhance anti-inflammatory drug efficacy. *ACS Appl. Mater. Interfaces* **2018**, *10*, 40378−40387.

(20) Ramirez, L. M. F.; Babin, J.; Boudier, A.; Gaucher, C.; Schmutz, M.; Er-Rafik, M.; Durand, A.; Six, J.-L.; Nouvel, C. First multi-reactive polysaccharide-based transurf to produce potentially biocompatible dextran-covered nanocapsules. *Carbohydr. Polym.* **2019**, *224*, No. 115153.

(21) Soliman, S. M. A.; El Founi, M.; Vanderesse, R.; Acherar, S.; Ferji, K.; Babin, J.; Six, J.-L. Light-sensitive dextran-covered PNBA nanoparticles to continuously or discontinuously improve the drug release. *Colloids Surf., B* **2019**, *182*, No. 110393.

(22) Man, T.; Zhu, X.; Chow, Y. T.; Dawson, E. R.; Wen, X.; Patananan, A. N.; Liu, T. L.; Zhao, C.; Wu, C.; Hong, J. S.; et al.

Intracellular Photothermal Delivery for Suspension Cells Using Sharp Nanoscale Tips in Microwells. *ACS Nano* **2019**, *13*, 10835−10844.
(23) Münkel, F.; Wefers, D. Fine structures of different dextrans assessed by isolation and characterization of endo-dextranase liberated isomalto-oligosaccharides. *Carbohydr. Polym.* **2019**, *215*, 296−306.
(24) Antoniou, E.; Tsianou, M. Solution properties of dextran in water and in formamide. *J. Appl. Polym. Sci.* **2012**, *125*, 1681−1692.
(25) Maia, J.; Evangelista, M. B.; Gil, H.; Ferreira, L. Dextran-based materials for biomedical applications. *Carbohydr. Appl. Med.* **2014**, 31−53.
(26) Almeida, J.; Ferreira, P.; Lopes, A.; Gil, M. Photocrosslinkable biodegradable responsive hydrogels as drug delivery systems. *Int. J. Biol. Macromol.* **2011**, *49*, 948−954.
(27) Damodaran, V. B.; Place, L. W.; Kipper, M. J.; Reynolds, M. M. Enzymatically degradable nitric oxide releasing S-nitrosated dextran thiomers for biomedical applications. *J. Mater. Chem.* **2012**, *22*, 23038−23048.
(28) Nguyen, M. K.; McMillan, A.; Huynh, C. T.; Schapira, D. S.; Alsberg, E. Photocrosslinkable, biodegradable hydrogels with controlled cell adhesivity for prolonged siRNA delivery to hMSCs to enhance their osteogenic differentiation. *J. Mater. Chem. B* **2017**, *5*, 485−495.
(29) Huh, M. S.; Lee, E. J.; Koo, H.; Yhee, J. Y.; Oh, K. S.; Son, S.; Lee, S.; Kim, S. H.; Kwon, I. C.; Kim, K. Polysaccharide-Based Nanoparticles for Gene Delivery. In *Polymeric Gene Delivery Systems*; Springer, 2017; pp 65−83.
(30) Zhang, J.-F.; Wang, Y.; Lam, M. L.; McKinnnie, R. J.; Claycomb, W. C.; Xu, X. Cross-linked poly (lactic acid)/dextran nanofibrous scaffolds with tunable hydrophilicity promoting differentiation of embryoid bodies. *Mater. Today Commun.* **2017**, *13*, 306−316.
(31) Pinho, A.; Fonseca, A.; Caseiro, A.; Pedrosa, S.; Amorim, I.; Branquinho, M.; Domingos, M.; Maurício, A.; Santos, J.; Serra, A. Innovative tailor made dextran based membranes with excellent non-inflammatory response: In vivo assessment. *Mater. Sci. Eng. C* **2020**, *107*, No. 110243.
(32) Gimlich, R. L. Fluorescent Dextran Clonal Markers. In *Methods in Cell Biology*; Elsevier, 1991; Vol. *36*, pp 285−297.
(33) Ren, K.; Ji, J.; Shen, J. Construction and enzymatic degradation of multilayered poly-L-lysine/DNA films. *Biomaterials* **2006**, *27*, 1152−1159.
(34) Murakami, T.; Okamoto, H.; Kim, H. Structural and functional changes in high-density lipoprotein induced by chemical modification. *Biomater. Sci.* **2015**, *3*, 712−715.
(35) Glover, J. C.; Petursdottir, G.; Jansen, J. K. Fluorescent dextran-amines used as axonal tracers in the nervous system of the chicken embryo. *J. Neurosci. Methods* **1986**, *18*, 243−254.
(36) Glover, J. Retrograde and anterograde axonal tracing with fluorescent dextran-amines in the embryonic nervous system. *Neurosci. Prot* **1995**, *30*, 1−13.
(37) Glover, J. C. Conjugated Dextran Amines as Intracellular Tracers for Visualizing and Manipulating Neurons. In *Dextran: Chemical Structure, Applications and Potential Side Effects*; Figgs, G. P., Ed.; Recent Trends in Biotechnology; Nova Publishers: Hauppauge, NY, 2014; pp 157−174.
(38) Habeeb, A. S. A. Determination of free amino groups in proteins by trinitrobenzenesulfonic acid. *Anal. Biochem.* **1966**, *14*, 328−336.
(39) Siegert, A. *Radiation Laboratory Report No. 465*; Massachusetts Institute of Technology: Cambridge, 1943.
(40) Kjøniksen, A.-L.; Nyström, B.; Tenhu, H. Characterisation of thermally controlled chain association in aqueous solutions of poly (N-isopropyl acrylamide)-g-poly (ethylene oxide): Dynamic light scattering. *Colloids Surf., A* **2003**, *228*, 75−83.
(41) Kjøniksen, A.-L.; Laukkanen, A.; Galant, C.; Knudsen, K. D.; Tenhu, H.; Nyström, B. Association in aqueous solutions of a thermoresponsive PVCL-g-C11EO42 copolymer. *Macromolecules* **2005**, *38*, 948−960.
(42) Chen, H.; Ye, X.; Zhang, G.; Zhang, Q. Dynamics of thermoresponsive PNIPAM-g-PEO copolymer chains in semi-dilute solution. *Polymer* **2006**, *47*, 8367−8373.
(43) Pan, C.; Cai, R.; Quacquarelli, F. P.; Ghasemigharagoz, A.; Lourbopoulos, A.; Matryba, P.; Plesnila, N.; Dichgans, M.; Hellal, F.; Ertürk, A. Shrinkage-mediated imaging of entire organs and organisms using uDISCO. *Nat. Methods* **2016**, *13*, 859−867.
(44) Liu, Y.; Chan-Park, M. B. A biomimetic hydrogel based on methacrylated dextran-graft-lysine and gelatin for 3D smooth muscle cell culture. *Biomaterials* **2010**, *31*, 1158−1170.
(45) Choi, H. S.; Yamamoto, K.; Ooya, T.; Yui, N. Synthesis of Poly (ε-lysine)-Grafted Dextrans and Their pH-and Thermosensitive Hydrogelation with Cyclodextrins. *ChemPhysChem* **2005**, *6*, 1081−1086.
(46) Rosca, I.; Petrovici, A. R.; Peptanariu, D.; Nicolescu, A.; Dodi, G.; Avadanei, M.; Ivanov, I. C.; Bostanaru, A. C.; Mares, M.; Ciolacu, D. Biosynthesis of dextran by Weissella confusa and its in vitro functional characteristics. *Int. J. Biol. Macromol.* **2018**, *107*, 1765−1772.
(47) Ioan, C. E.; Aberle, T.; Burchard, W. Structure properties of dextran. 2. Dilute solution. *Macromolecules* **2000**, *33*, 5730−5739.
(48) Hanselmann, R.; Burchard, W.; Lemmes, R.; Schwengers, D. Characterization of DEAE-dextran by means of light scattering and combined size-exclusion chromatography/low-angle laser light scattering/viscometry. *Macromol. Chem. Phys.* **1995**, *196*, 2259−2275.
(49) Rotureau, E.; Chassenieux, C.; Dellacherie, E.; Durand, A. Neutral polymeric surfactants derived from dextran: A study of their aqueous solution behavior. *Macromol. Chem. Phys.* **2005**, *206*, 2038−2046.
(50) Carpenter, J. F.; Crowe, J. H. An infrared spectroscopic study of the interactions of carbohydrates with dried proteins. *Biochemistry* **1989**, *28*, 3916−3922.
(51) Wolkers, W. F.; van Kilsdonk, M. G.; Hoekstra, F. A. Dehydration-induced conformational changes of poly-L-lysine as influenced by drying rate and carbohydrates. *Biochim. Biophys. Acta, Gen. Subj.* **1998**, *1425*, 127−136.
(52) van Dijk-Wolthuis, W.; Franssen, O.; Talsma, H.; Van Steenbergen, M.; Kettenes-Van Den Bosch, J.; Hennink, W. Synthesis, characterization, and polymerization of glycidyl methacrylate derivatized dextran. *Macromolecules* **1995**, *28*, 6317−6322.
(53) Stenekes, R.; Talsma, H.; Hennink, W. Formation of dextran hydrogels by crystallization. *Biomaterials* **2001**, *22*, 1891−1898.
(54) Ioan, C. E.; Aberle, T.; Burchard, W. Structure properties of dextran. 3. Shrinking factors of individual clusters. *Macromolecules* **2001**, *34*, 3765−3771.
(55) Burchard, W. Static and dynamic light scattering from branched polymers and biopolymers. *Light Scattering Polym.* **1983**, 1−124.
(56) Burchard, W. Solution Properties of Branched Macromolecules. In *Branched Polymers II*; Springer, 1999; pp 113−194.
(57) Kirkwood, J. G.; Riseman, J. The intrinsic viscosities and diffusion constants of flexible macromolecules in solution. *J. Chem. Phys.* **1948**, *16*, 565−573.
(58) Mirsharghi, S.; Knudsen, K. D.; Bagherifam, S.; Nyström, B.; Boas, U. Preparation and self-assembly of amphiphilic polylysine dendrons. *New J. Chem.* **2016**, *40*, 3597−3611.
(59) Fritzsch, B. Fast axonal diffusion of 3000 molecular weight dextran amines. *J. Neurosci. Methods* **1993**, *50*, 95−103.

https://doi.org/10.1021/acsabm.1c00544
ACS Appl. Bio Mater. 2021, 4, 6832−6842